ELSEVIER

Tectonophysics 329 (2000) 61–78

TECTONOPHYSICS

www.elsevier.com/locate/tecto

Seismic tomography with local earthquakes in Costa Rica

V. Sallarès[a,*], J.J. Dañobeitia[a], E.R. Flueh[b]

[a]*Institute of Earth Sciences Jaume Almera - CSIC, c/Lluïsa Solé i Sabarís, s/n, 08028 Barcelona, Spain*
[b]*Research Center for Marine Geosciences GEOMAR, Kiel, Germany*

Received 26 May 1999; accepted 21 October 1999

Abstract

The Costarican isthmus is located at the western limit of the Caribbean oceanic plateau, where the Cocos plate subducts along the Middle American Trench. This plate shows strong lateral variations in its morphology and structure. The main objective of this study is to investigate the effects of subduction-related magmatism as a function of morphology and structure of the subducting plate, by performing a simultaneous inversion of the 3-D crustal velocity field and hypocenter locations from local earthquakes. For that, we used the traveltimes of P-waves first arrivals from more than 5000 events, recorded at the Costarican seismic networks between 1991 and 1998. In order to prevent data and modeling inaccuracies, we followed an inversion scheme consisting of four steps. (1) Selection of an adequate data subset for tomographic inversion, (2) estimation of the best reference 1-D model, (3) determination of the finest parameterization and (4) evaluation of resolution. The results show that the uppermost levels of the crust (0–6 km) are consistent with geology, since the velocity anomalies reflect the most meaningful geological features observed in the surface. Below these levels (6–20 km deep), we found two different zones separated by a SW–NE seismic alignment. The northern part is characterized by a highly heterogeneous velocity field and is seismically active, while the southern part is much more homogeneous and practically inactive. Moreover, the northern part shows a certain accumulation of low velocity material within the upper mantle. We suggest and illustrate that the structural differences between the northern and southern zones can be a consequence of the differences on the geometry and structure of the subducting slab.

Keywords: seismic tomography; hypocenter; tomographic inversion

1. Introduction

The formation of oceanic plateaus and hotspots, related to intraplate magmatism induced by mantle plumes, and the build up of island arcs, as a result of subduction-related magmatism, are processes that contribute to the preservation of oceanic lithosphere and to the continental growth. The magma produced by these processes modifies and substantially thickens the oceanic crust, preventing its subduction and favoring its accretion to the active continental margins. The study zone is well suited to investigate this kind of magmatic processes, since it has been affected by a mantle plume (origin of the plateau) and even shows a subduction zone (Duncan and Heargraves, 1984; Burke, 1988; Donnelly, 1994). The morphology and structure of the Cocos plate and the geometry and dynamics of subduction along the different parts of the study zone are well established by the works of many authors (Burbach et al., 1984; Protti et al., 1995; Von Huene et al., 1995; Ye et al., 1996; Stavenhagen

* Corresponding author. Present address: IRD-Geosciences Azur, B.P. 48-06235, Villefranche-sur-mer Cedex (France). Tel.: (33)4937649; fax: (33)493763768.
E-mail address: vsallares@ija.csic.es (V. Sallarès).

0040-1951/00/$ - see front matter
PII: S0040-1951(00)00188-8

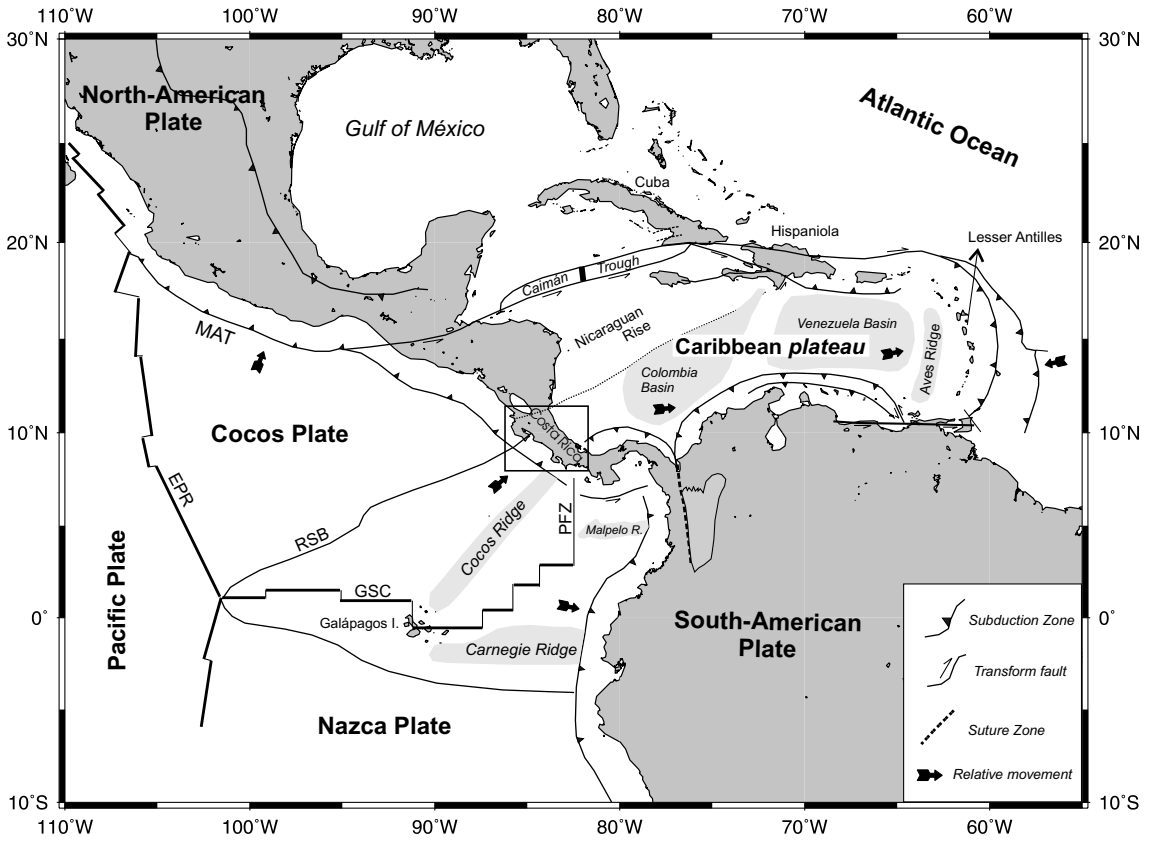

Fig. 1. Regional tectonic map of the study zone (box). The most meaningful tectonic events are indicated. Abbreviations — MAT: Middle American Trench; RSB: Rough-Smooth boundary; ENFZ: East Nicoya Fracture Zone; PFZ: Panamá Fracture Zone; EPR: East Pacific Rise; GSC: Galápagos Spreading Center.

et al., 1998). These studies have shown that the northern half of the isthmus is characterized by the subduction of a thin and smooth oceanic crust (6–7 km thick) with a dip angle of about 60°, and the deepest subduction-related earthquakes are located below 150 km. In contrast, the southern half shows the subduction of a rough and thickened oceanic crust (up to 11–12 km), which main morphological expression corresponds to the Cocos Ridge. The dip angle of this crustal section is considerably lower, and the deepest earthquakes are located above 70 km. These structural differences are also reflected inland. The northern half is seismically active and shows an active volcanic arc, while the southern half is less active and exhibits a volcanic gap. In spite of these observations, little is known about the crustal structure of the isthmus. Most of the structural information comes from seismic refraction profiling (Goedde et al., 1997; Sallarès et al., 1999). These studies have demonstrated that the crust of the isthmus is about 40 km thick, which is practically two times the averaged thickness of the Caribbean plateau. This suggests that the Costarican isthmus has been extensively affected by subduction-related magmatism since it was established in the Late Cretaceous. However, it is necessary to obtain 3-D velocity field information in order to determine more accurately the influence of subduction in the different parts of the isthmus. This study has been carried out to fulfil this lack of information.

2. Tectonic setting

The Costarican isthmus is located at the boundary

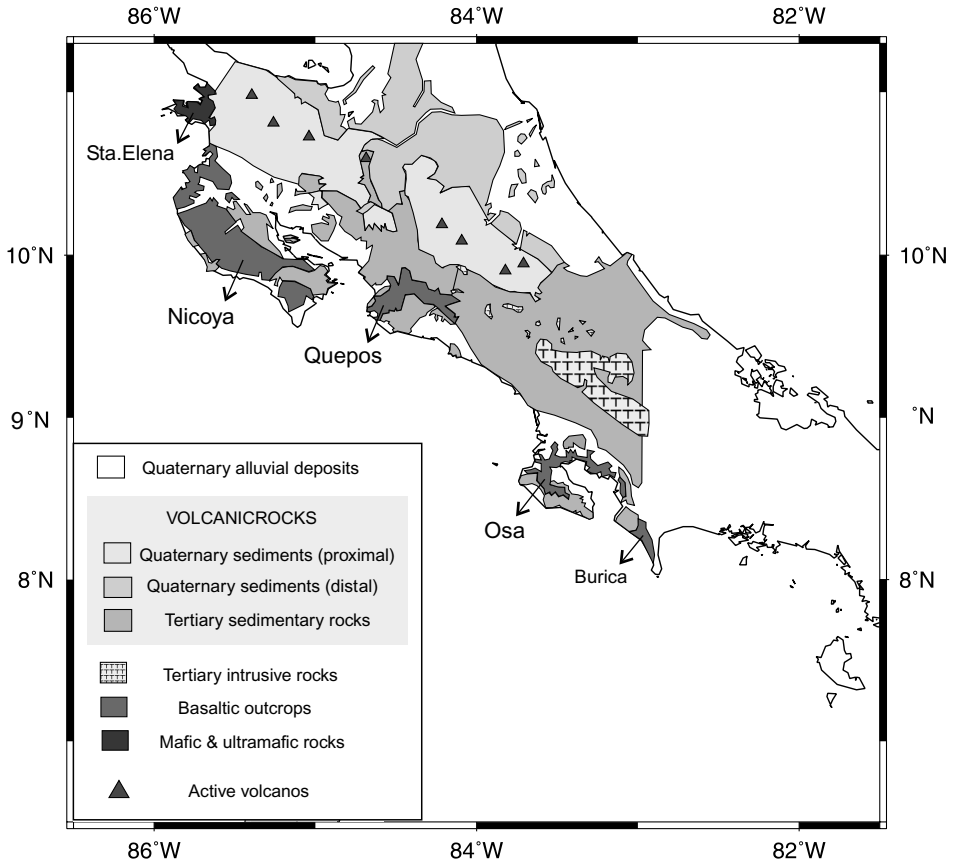

Fig. 2. Geological map of the Costarican isthmus (modified from Tournon and Alvarado, 1997).

between two tectonic plates. The Caribbean plate, which includes the isthmus sensu stricto and extends to the East until the Lesser Antilles island arc, and the Cocos plate, which subducts along the Middle American Trench (MAT) from northern Guatemala to southern Costa Rica (Fig. 1).

The Cocos plate is generated at two different zones, the East Pacific Rise (EPR) in the West, and the Galápagos Spreading Center (GSC), in the South. The boundary between the plate created at the EPR and at the GSC was for a long time believed to be represented by the Rough-Smooth Boundary (RSB) (Hey, 1977). However, more recent work with better magnetic coverage (Barckhausen et al., 1998), swath bathymetry (Von Huene et al., 1999) and dating (Werner et al., 1999), placed this transition slightly northward, at the middle of the Nicoya Peninsula. The plate created at the EPR is typically oceanic, while the plate created at the GSC has been overthickened by igneous material extruded at the Galápagos hotspot (Fig. 1). The Cocos Ridge traces the path of the Galápagos hotspot through the Cocos plate. According the structural differences of the Cocos plate, three morphological provinces have been distinguished (Fig. 2) (Von Huene et al., 1995). The northern one subducts under the Nicoya Peninsula, and corresponds to a typical subduction zone, having an associated volcanic arc with recent phases of calc-alkaline magmatism (Kussmaul et al., 1994). The central part (the Quepos segment) subducts south of the RSB, where the crust has been slightly thickened by Galápagos hotspot-derived material (Ye et al., 1996). This zone shows the existence of numerous seamounts (Fisher, 1961), some of which have been accreted on the margin since the Miocene (Hauff et al., 1997). Nevertheless, the geometry of sudbduction

is similar to the northern segment, having also an associated volcanic arc. The dip angle is slightly lower than in the Nicoya Peninsula (Protti et al., 1995). Finally, the narrow shelf off the southern part (adjacent to the Osa Peninsula) corresponds to the subduction of the Cocos Ridge. The differences between this segment and the central and northern ones are remarkable. Thus, the margin shows the presence of allocthonous igneous terrains which have been accreted in distinct phases (Berrangé and Thorpe, 1988), the subduction angle is much lower (Protti et al., 1995) and there are not current episodes of volcanism. One of the main questions concerning the recent tectonic evolution of the Cocos plate is the history of subduction of the Cocos Ridge. Most of the authors postulated that the onset of the subduction was caused by the irruption of the Panamá Fracture Zone (PFZ, Fig. 1) in the Upper Miocene. This event moved the boundary Nazca-Cocos towards the northwest, placing the triple point Nazca-Cocos-Caribe near the Nicoya Peninsula (Gardner et al., 1992) and yields the fracture of the Cocos Ridge in two segments. The northern segment moved away to the south, forming the current Malpelo Ridge. The southern one was displaced to the north, and begun to subduct beneath the isthmus about 1 Ma ago (Longsdale and Klitgord, 1978), inducing the tectonic uplift of the Osa Peninsula (Corrigan et al., 1990).

The tectonic evolution of the Costarican isthmus is more controversial. Most of the recent geochemical (Sinton et al., 1997, 1998; Alvarado et al., 1997), geological (Donnelly, 1994) and geophysical (Bowland and Rosencrantz, 1988; Sallarès, 1999) data suggest that the basement of the isthmus represents the westernmost end of the Caribbean plateau. Thus, the igneous outcrops of the Nicoya Complex (Fig. 2) and most of the marginal wedge would represent part of this extrusive basement (Hinz et al., 1996; Sallarès et al., 1999).

The Caribbean plateau is thought to be formed during Late Cretaceous, as a result of the initial phase (the 'head phase') of a mantle plume which on a later stage originated the Galápagos hotspot (Duncan and Heargraves, 1984; Richards et al., 1989; Hill, 1993). Once integrated in the overlying lithosphere, the Caribbean plateau derived towards NE, going into the South American and North American plates and colliding with the Lesser Antilles island arc 75–80 Ma ago (Burke, 1988; Pindell and Barrett, 1990). The suture between the plateau and the island arc induced the onset of subduction beneath the isthmus and the first phases of associated andesitic volcanism during the Campanian (Lundberg, 1991; Kussmaul et al., 1994). Hence, the structural differences between the plateau and the isthmus are thought to be caused by the magmatism which developed the volcanic arc (Sallarès, 1999). An alternative description suggests that part of the Costarican isthmus represents a fragment of oceanic crust or the remnant of an island arc as old as Jurassic. This arc would have been originated independently to the Caribbean plateau, being accreted afterwards in its western margin (Wildberg, 1984; Frisch et al., 1992). This hypothesis is based on the biostratigraphic ages of the radiolarian cherts (100–150 Ma), which separate apparently the Upper and Lower parts of the Nicoya Complex. However, recent $^{39}Ar/^{40}Ar$ dating (Sinton et al., 1997) have demonstrated that both the Upper and Lower parts of the Nicoya Complex have approximately the same age (~88 Ma). Thus, the radiolarian cherts are interpreted as a remnant of the sedimentary cover of the pre-existing oceanic crust, which was intruded and deformed by the extrusion of the basement in the Late Cretaceous (Gursky, 1988; Donnelly, 1994).

3. Selection of the data set

The initial data set considered in this study is composed by 30028 first arrivals of P-waves from 5166 local earthquakes that occurred in Costa Rica between 1991 and 1998. The stations of two national seismic networks, which operate independently in Costa Rica, recorded these events. The first one is composed by 32 stations and is controlled and maintained by the Observatorio Vulcanológico y Sismológico de Costa Rica (OVSICORI) and the Universidad Nacional (UNA). About 30 stations from the Instituto Costarricense de Electricidad (ICE) and the Universidad de Costa Rica (UCR) constitute the second one. For a more detailed description of both seismic networks, see Güendel et al. (1989) and Colombo (1995). Moreover, several local seismic networks have operated in Costa Rica in distinct microseismicity studies during the last years, mainly around the volcanic arc.

Nowadays, the data from both fix and temporary

networks (81 stations in total) are being reinterpreted and compiled by the Centro de Prevención de Desastres Naturales de América Central (CEPREDENAC). This institution provided us with a data set including the hypocentral locations and first arrival readings from about 3300 events, recorded between 1991 and 1995. The rest of data, which includes ~1900 events recorded between 1991 and 1998, were provided by the ICE-UCR, and they were recorded only by the seismic stations from this institution.

The seismic phases were classified following a standard criteria of quality control. These criteria are used to assign a weight to each observation, which is inversely proportional to the estimated reading errors. A significant number of these 5166 events (Fig. 3a) remain poorly locatable, mainly due to the low number of observations (5.8 in average) and to the gap between rays (>180°). Therefore, it is necessary to select an adequate data set for the tomographic inversion, which has to guarantee convergence and stability in the inversion of hypocentral coordinates. Generally, the inclusion of S-waves is considered as a useful condition to improve the hypocentral parameters determination (Gomberg et al., 1990). However, our data set is subject to important uncertainties in the identification of S-waves, since most of the geophones are only of vertical component. Thus, we consider alternative constraints to keep the number of data large enough. The restrictions in this step are as follows: (1) a minimum of 10 readings of P-phases for each event; (2) the maximum gap is less than 180°; (3) the root mean square (rms) is lower than 2.5 s. Similar restrictions have been successfully used in several tomographic studies (Solarino et al., 1997; Dañobeitia et al., 1998). The resulting data set after this step includes 7953 P-observations from 583 local earthquakes, which locations are shown in Fig. 3b. This data set was then used in the tomographic inversion.

4. Best reference 1-D model

The importance of an adequate reference velocity model, prior to 3-D tomographic inversion, has been repeatedly mentioned by many authors (Kissling, 1988; Thurber, 1992; Kissling et al., 1994). This is due to the non-uniqueness of the solution of the linearized inverse problem. This trouble has frequently been underestimated in a number of tomographic studies, leading to blunders and biases on the results. In this study, we determine the reference model following a procedure similar to that of Kissling et al. (1994). This procedure consists of checking the space of parameters, considering different 1-D initial models with a varying number, thickness and initial velocity of layers. These initial models are built according to the structural information from seismic refraction. Hence, the velocity and thickness of the different layers should be consistent with those obtained from the refraction seismic records. The a priori information that we considered includes the 1-D velocity-depth profile obtained by Matumoto et al. (1977) and a 2-D velocity-depth model from northern Costa Rica (Sallarès et al., 1999). The initial models were then used to perform a 1-D inversion of the velocity and hypocentral parameters and station corrections, using the VELEST algorithm (Kissling, 1988). The first step includes the earthquakes relocation within each initial model, which allows homogenizing the whole data set with respect to these models, avoiding biases and inconsistencies between the data subsets of dissimilar origin.

The best reference 1-D model (or minimum 1-D model), selected among all the final 1-D models, must satisfy the following conditions: (1) minimizes the averaged residual time; (2) has to be robust (weakly dependent on the initial model); (3) consistent with the a priori information. Our best reference 1-D model is shown in Fig. 4. The range of convergence of this model has been estimated by trial and error, varying the velocities of the initial model and looking at their effects in the final model. As shown in Fig. 5a and b, this model reduces by about 35% the residual times with respect to the initial model of Matumoto et al. (1977). This suggests that this model describe more accurately the velocity field of the Costarican isthmus. Moreover, we also evaluate the internal consistency of the data set. For that, we consider two independent data subset of 281 events, randomly distributed within the study zone. Then, we have inverted the velocity field for each of them, considering identical initial models. The results of these two inversions are very similar, being also compatible (± velocity uncertainties) with the best reference 1-D model of Fig. 4.

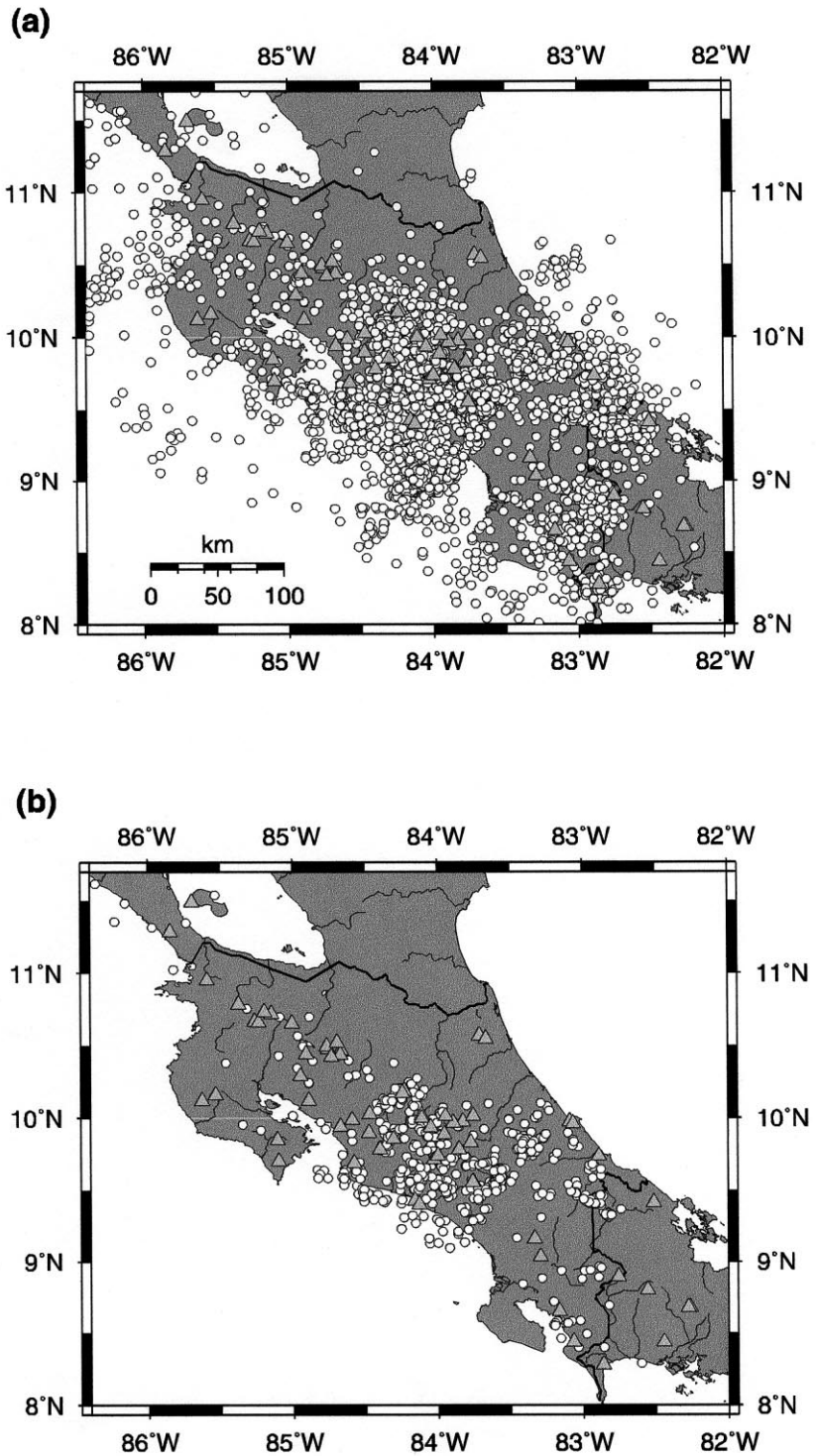

Fig. 3. Location map of the local earthquakes recorded by all the stations that operated in Costa Rica between 1991 and 1998. Panel (a) corresponds to the 5166 events from the initial data set. Panel (b) corresponds to the 583 well locatable events used for tomographic inversion.

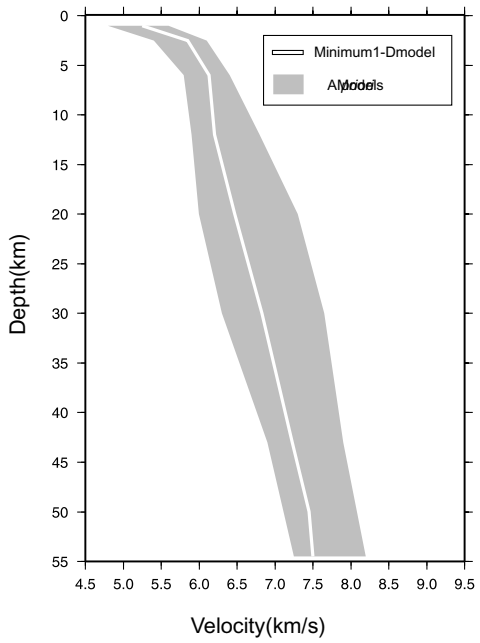

DEPTH	VELOCITY	ERROR	RANGE	NºEVENTS
0-2	4.8-5.8	-	-	120
2-6	5.99	<0.05	±0.75	90
6-12	6.20	<0.05	±0.75	91
12-20	6.31	<0.05	±0.75	71
20-30	6.74	<0.1	±0.5	38
30-43	7.10	<0.1	±0.5	42
43-65	7.47	<0.05	±0.6	66
65-120	7.8-8.1	-	-	58
120-	8.1-8.4	-	-	7

Fig. 4. Velocity-depth profile corresponding to the best reference 1-D model. Velocity uncertainties (km/s), the range of convergence (km/s), and the number of events within each layer are also indicated.

These outcomes show that we can estimate the averaged seismic velocities of the study zone, with an error of less than 0.1 km/s, for a range of depths between ~2 and 65 km. The velocities of the uppermost (<2 km) and lowermost (>65 km) layers are not well constrained, thus we fixed them during the inversion accordingly to the a priori information. Nevertheless, these velocities do not have a major influence on the velocities of the rest of the layers (see Fig. 4). Thus, we found that the crust of the isthmus is characterized by a uniform velocity-depth gradient, without abrupt velocity contrasts. This is in agreement with refraction seismic, since the record sections do not show prominent intracrustal reflections (Sallarès et al., 1999). In general terms, this velocity model is very similar to the refraction ones at upper and mid crustal levels (<30 km depth), but differs substantially at the lower part of the crust (30–43 km) and, especially, at upper mantle level (43–65 km). The good control of seismic velocities at these depths is assured by the existence of 173 deep earthquakes (>30 km) in the data set. Hence, velocities at the lower part of the crust range between 7.05 and 7.15 km/s, while the velocities within the upper mantle are notably low (7.4–7.5 km/s). In contrast, velocities previously inferred from refraction seismic were much higher within the upper mantle (8.0–8.1 km/s). However, a recent reinterpretation of the refraction data from the northern profile showed that the inclusion of lower velocities within the upper mantle is also justified by these data, since the calculated synthetic seismograms fit better the amplitudes of the deep seismic phases (Sallarès, 1999).

5. Parameterization of the model

The finest parameterization of the velocity field was determined estimating the sensibility of our data set in the distinct parts of the study zone. For that, we built some different models, varying the number and distribution of nodes within each layer. Then we performed a checkerboard test for each of them, keeping the locations and number of observations of the local earthquakes, and inserting velocity anomalies of ±5% with respect to the best reference 1-D model. The synthetic traveltimes through the 'checkerboard models' were computed using the algorithm of Um

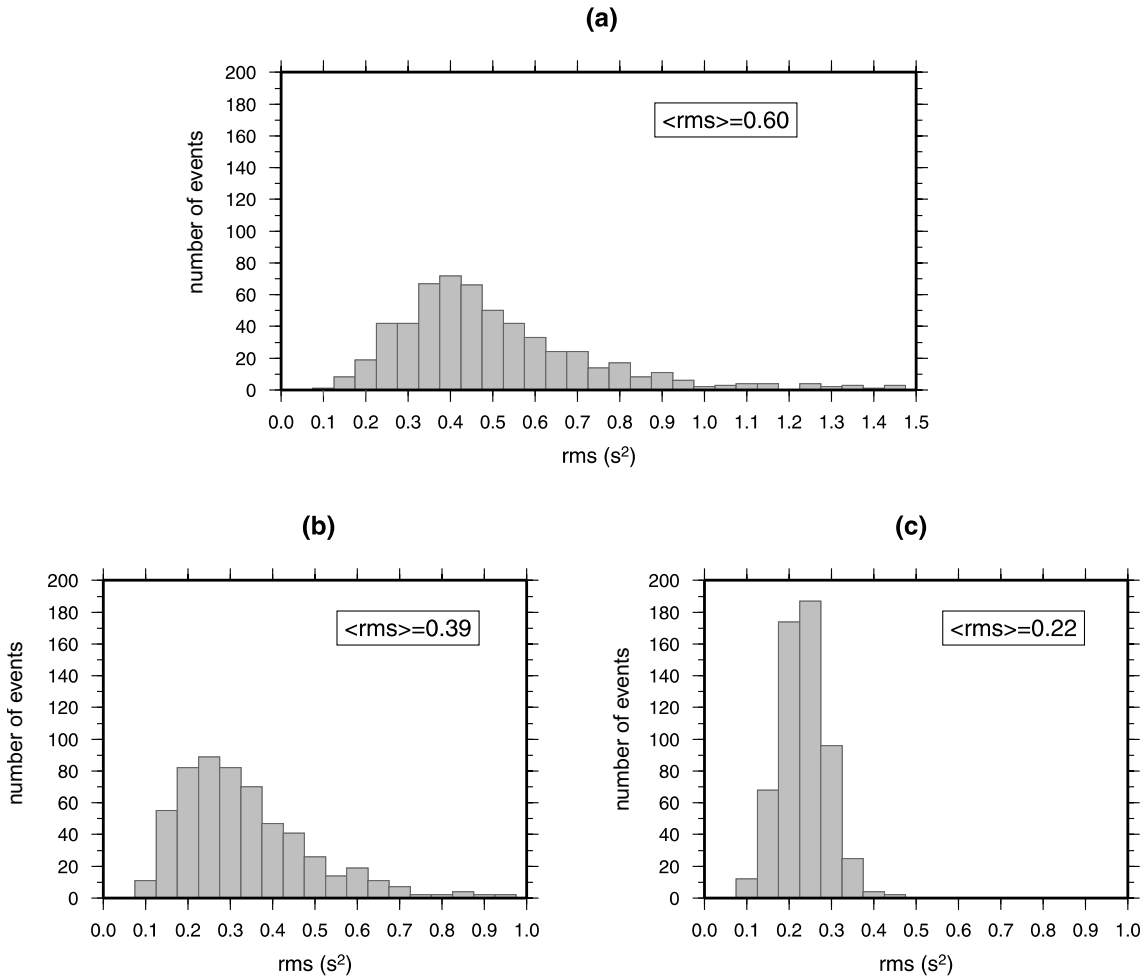

Fig. 5. Histogram of traveltime residuals (s^2) obtained with the 1-D velocity model of Matumoto et al. (1977) (a), the best reference 1-D model of Fig. 4 (b), and the final 3-D model (c).

and Thurber (1987). In order to improve fidelity of the results we added random errors to the observations, proportional to the estimated reading uncertainties. Afterwards, a 3-D inversion was performed considering the best reference 1-D model as initial model, and using the SIMULPS12 algorithm of tomographic inversion (Thurber, 1983). Fig. 6 shows the results of one of these inversions, and Fig. 7 shows the distribution of nodes corresponding to the velocity model. This is the model we used thereafter in the inversion with the 'real' data set.

The checkerboard test shows that the sensibility of the data set varies considerably depending on the depth of the layers. The best approximation is found at the intermediate layers (2–4; 2.5–20 km depth), where the sign of the velocity anomalies is correctly recovered in a wide zone of central and southern Costa Rica. The uppermost layer shows a scattered pattern, while smearing is evident in the bottommost ones. These effects are caused by the geometry of the rays. Most of the rays crossing the uppermost layer are subvertical, which means that the well-resolved anomalies are constrained immediately below the receivers. In contrast, rays crossing the bottommost layers are subhorizontal, so they only contain relative information on this direction and thus the resolution is much lower. Another meaningful effect is that inverted velocity anomalies are systematically lower

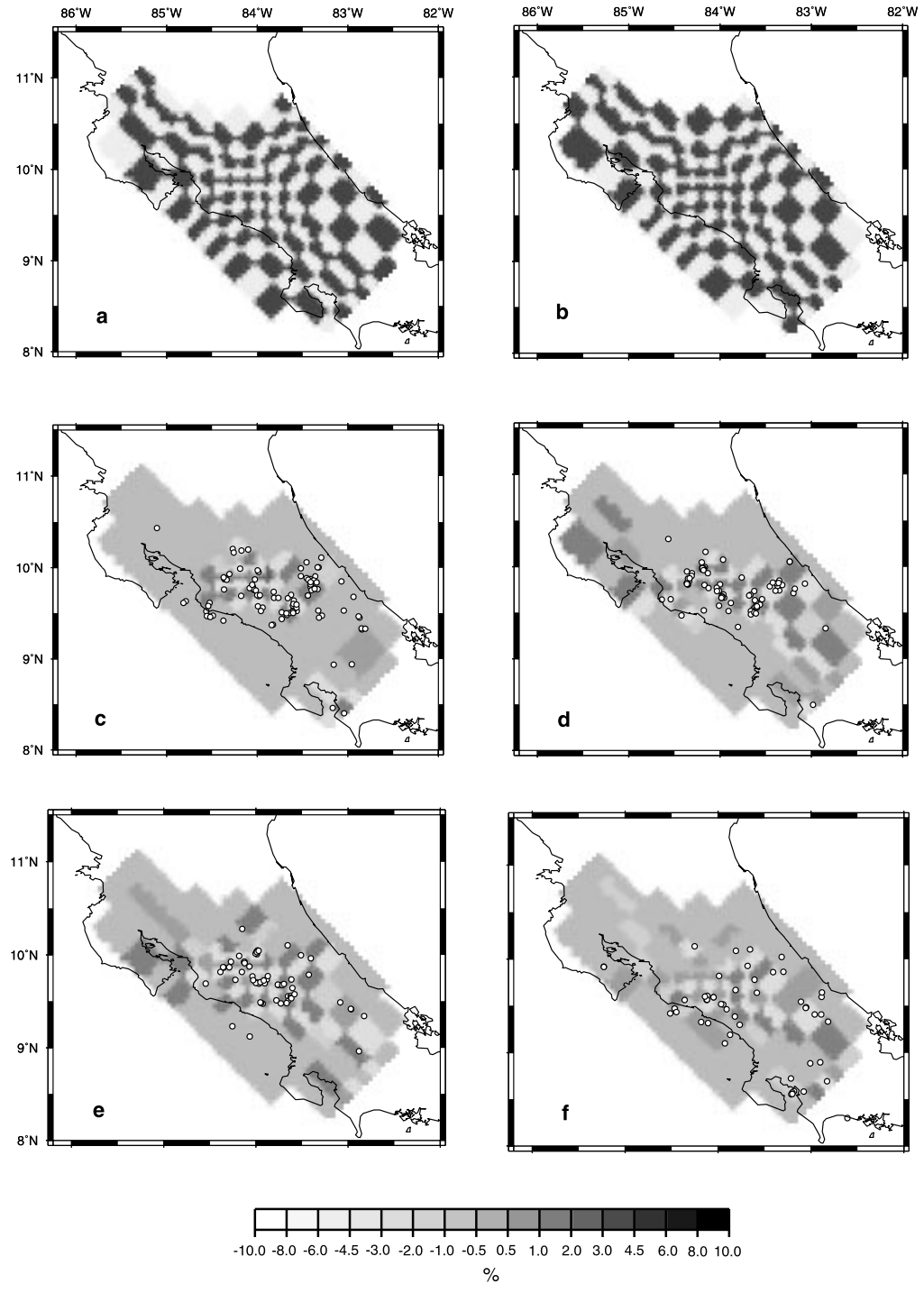

Fig. 6. Results of the checkerboard test for Layers 1 (0–2 km depth, panel c), 2 (2–6 km depth, panel d), 3 (6–12 km depth, panel e) and 4 (12–20 km depth, panel f). Velocity deviations are indicated in % with respect to the best reference model of Fig. 4. Panels a and b show the synthetic model (odd and even layers) used for calculation of traveltimes. Dots show position of local earthquakes within each layer.

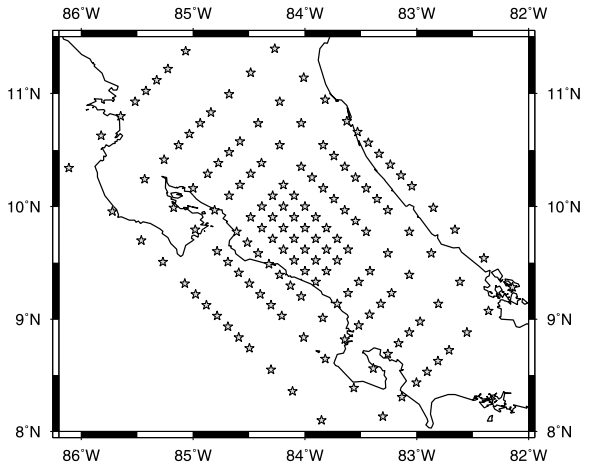

Fig. 7. Nodes distribution within each layer used for 3-D tomographic inversion.

(up to 50%) than those considered in the synthetic model. This effect is caused by the coupling between velocity and hypocentral parameters in the simultaneous inversion problem (Thurber, 1992).

6. 3-D inversion and resolution analysis

One of the major difficulties concerning local earthquakes tomography is that the direct problem (i.e. the traveltime calculation) is non-linear. Fortunately, the effects of non-linearity are only of second order, as Fermat's Principle demonstrates. This prompts that most of the existing inversion techniques consider a first order approximation of the direct problem, and invert it following an iterative scheme. In this study we used the iterative inversion method of Thurber (1983), which finds the solution minimizing by least squares a measure of the discrepancy between calculated and observed travel times (i.e. the residual times). In order to diminish errors in the solution induced by errors in the data set, the observations are weighted according to their quality (see 'Selection of the data set'). A parameter separation technique (velocity/hypocenter parameters) is used to make the matrix of coefficients (A in Eq. (1)) smaller (Pavlis and Booker, 1980). Moreover, a damping factor is incorporated to the normal equations. The value of the damping factor indicates the relative importance of the change on the model parameters (i.e. the a priori information) with respect to the data variance (i.e. information contained in the data set), and the optimal value is chosen by trade-off analysis (Eberhart-Phillips, 1986). The formal expression of the solution is then the next:

$$\Delta m = (A^{\mathrm{T}} C_d^{-1} A + \epsilon^2 I)^{-1} A^{\mathrm{T}} C_{\mathrm{d}}^{-1} \delta T \quad (1)$$

where Δm is the vector of velocity parameters variation, A the partial derivatives matrix (traveltime with respect to velocity parameters), C_{d} the a priori covariance data matrix (diagonal), ϵ the damping factor, δT the vector of residual times and I the identity matrix.

The solution given by Eq. (1) is subject to data (C_{d}) and modeling (ϵ) inaccuracies. Thus, the solution is not exact, so assessments of the outcome fidelity, before their interpretation, are required. This estimation is carried out following a scheme that we used in a previous study (Dañobeitia et al., 1998). This scheme incorporates the calculation of some control parameters, such as the diagonal elements of the resolution matrix (R), the derivative weight sum (DWS) and the number of hits (NH) for each node (Fig. 8). The well-resolved zones are then selected by comparing qualitatively the outcomes from this analysis and those from the checkerboard test (Fig. 7). This procedure allows to define a systematic procedure to discern between well resolved ($R > 0.4$, DWS > 40 and NH > 10) and bad resolved ($R < 0.4$ or DWS < 40 or NH < 10) nodes. The results of the 3-D inversion, for the well-resolved zones within Layers 1–6, are shown in Fig. 9. This model reduces the averaged residuals in about 50% with respect to the best reference 1-D model (see Fig. 5b and c).

7. Results

Layers 1 (0–2 km) and 2 (2–6 km) show a similar velocity field, in which the well-resolved zones are constrained at the central and southern parts of the Costarican isthmus (Fig. 8a and b). The velocity field within these zones is characterized by *large* (~100 km) and conspicuous (±10%) velocity anomalies. Most of these anomalies can be related with the most meaningful geological features observed in the surface (see geological map in Fig. 2). Hence, the lowermost velocities are obtained below the volcanic arc, where the most recent volcanic products are concentrated. This anomaly is surrounded by relatively high velocities, which depict

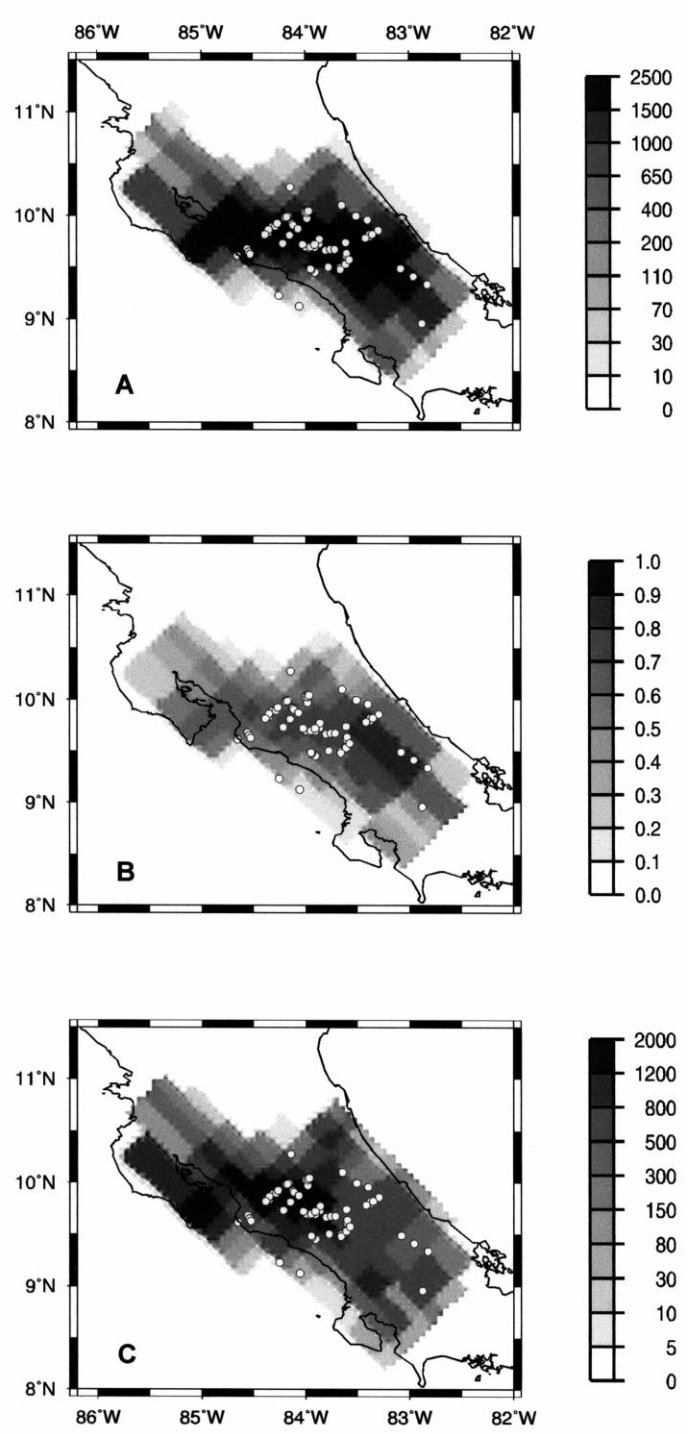

Fig. 8. Control parameters obtained for Layer 3 (6–12 km depth). (a) Diagonal element of the resolution matrix (R). (b) Derivative Weight Sum (DWS). (c) Number of hits (NH). The well-resolvable zones are defined by $R > 0.4$, DWS > 40, NH > 10. Event locations within this layer are also displayed.

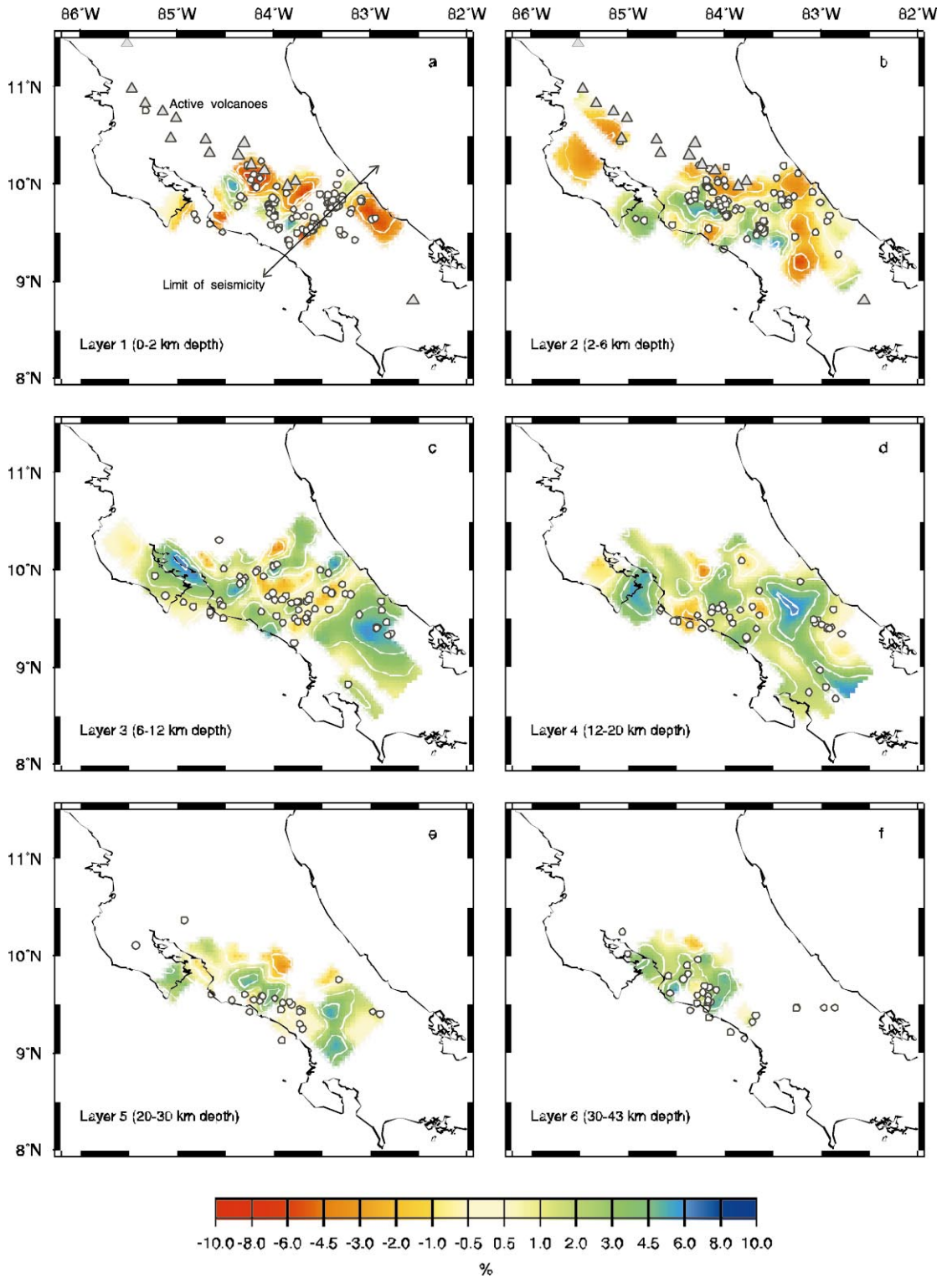
86°W
85°W
84°W
83°W
82°W
11°N
10°N
9°N
8°N
a
Active volcanoes
Limit of seismicity
Layer 1 (0-2 km depth)
b
Layer 2 (2-6 km depth)
c
Layer 3 (6-12 km depth)
d
Layer 4 (12-20 km depth)
e
Layer 5 (20-30 km depth)
f
Layer 6 (30-43 km depth)
-10.0 -8.0 -6.0 -4.5 -3.0 -2.0 -1.0 -0.5 0.5 1.0 2.0 3.0 4.5 6.0 8.0 10.0
%

the extension and geometry of the Tertiary volcanic materials, which cover most of the isthmus's basement (Tournon and Alvarado, 1997). These materials are more consolidated than the recent ones, thus it is normal to find low velocities around the volcanic arc (ashes) and higher ones as we move away from the arc. Low velocity anomalies are also obtained in the Caribbean coast (Layers 1 and 2) and in the northern part of the Nicoya peninsula (Layer 2). These anomalies are probably related with the deposits of alluvial Quaternary materials and volcanic sediments, which can be as thick as 4 km in the Tempisque basin (northern Nicoya) (Astorga et al., 1991). Another anomaly of relative high velocity is obtained southeast from the Nicoya Peninsula (Layer 2). We associate this anomaly with the extrusive basement of the isthmus, which outcrops in the Nicoya Complex (Alvarado et al., 1997). The contribution of the high velocities characterizing the basement is probably reflected also in most of the high velocity anomalies inverted throughout the whole layer. In Layer 2, it is also identified a conspicuous large-scale low velocity anomaly trending N–S in the southern half of the isthmus. This anomaly is difficult to correlate to any geological feature, though we suggest that it could be the expression of a suite of intrusive bodies which have been described in the southern half (Kussmaul et al., 1994).

As shown in Fig. 9a and b, almost all the local seismicity within Layers 1 and 2 is constrained at the central part of the isthmus. The boundary between the seismically active northern part and the practically inactive southern part is marked by a SW–NE seismic alignment, which is located slightly to the SE from the end of the active volcanic arc. This behavior of the local seismicity is also representative of the intermediate Layers 3 (6–12 km) and 4 (12–20 km) (Fig. 9c and d), where a similar seismic alignment separates both the active and less active parts of the isthmus. Therefore, we suggest that the intracrustal seismicity in the northern part can be mostly related with magmatic activity, while the abrupt decreasing of seismicity in the southern part could be partly explained by the lack of current volcanism.

The well-resolved zones within intermediate and deep Layers 3–6 are progressively smaller because of resolution diminishing (Fig. 9c–f). However, they are large enough within Layers 3–5 (6–30 km in total) to identify the main properties of the velocity field. The best resolved layer is number 3 (6–12 km) (Fig. 9c). The appearance of its velocity field is notably different to that obtained within the overlying layers, since the velocity anomalies do not reflect the geological features. More likely, two zones showing quite different characteristics define it. The first zone can be very well correlated with the seismically and magmatically active northern part, and is characterized by a sequence of low- and high- small-scale ($\lambda < 20$ km) velocity anomalies. In contrast, the second one is confined in the inactive southern part, showing a much more homogeneous velocity field. This part is defined by a unique relatively high velocity anomaly. Although less evident, the behavior of the velocity field within Layer 4 (12–20 km) is basically the same as for Layer 3 (Fig. 9d). Thus, it shows a seismically active and highly heterogeneous northern half and a more homogeneous and less active southern half. Layer 5 (20–30 km) shows a slightly different behavior (Fig. 9e). Seismicity is not only constrained within the northern half of the isthmus. Moreover, the events within this part are mostly located near the margin, which indicates that they are probably related with the subduction of the Cocos plate. A heterogeneous velocity field also characterizes the velocity field, with high velocities near the margin and lower velocities onshore. In the southern part, there is certain activity trending approximately S–N, which can be correlated with a high velocity anomaly trending in the same direction. We suggest that this velocity anomaly and the associated seismicity could be related with the subduction of the Cocos Ridge, but this seismicity is scarce and results are not sufficiently well constrained to confirm this hypothesis. The only well-resolved zone within Layer 6 (30–43 km) is located beneath the margin of the central part, where most of the seismicity take place (Fig. 9f). Consequently, it is not possible to

Fig. 9. Final results for Layers 1 (0–2 km depth, panel a), 2 (2–6 km depth, panel b), 3 (6–12 km depth, panel c), 4 (12–20 km depth, panel d), 5 (20–30 km depth, panel e) and 6 (30–43 km depth, panel f). Velocity deviations are indicated in percent with respect to the best reference model of Fig. 4. Each image shows only the well-resolved zones. Dots show the hypocentral locations within each layer.

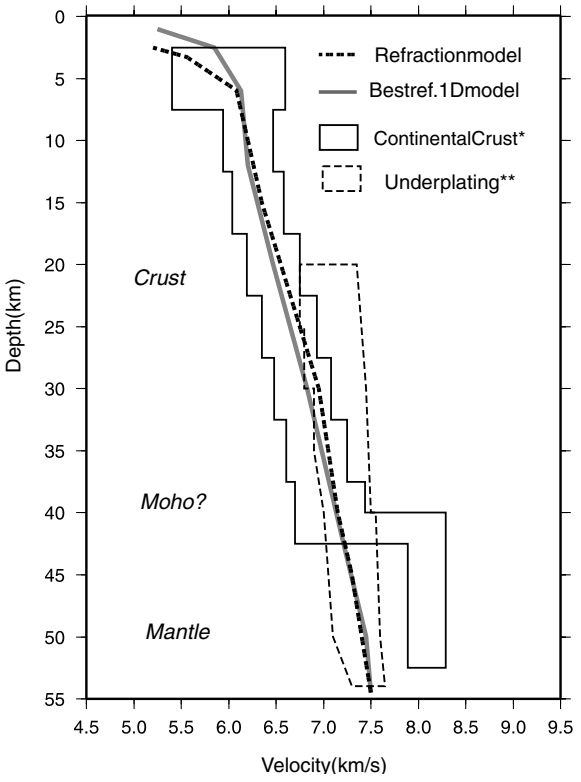

Fig. 10. 1-D velocity-depth profiles from the Costarican isthmus. The solid line corresponds to the best reference 1-D model (Fig. 4), and the dashed line is taken from a 2-D velocity-depth model from northern Costa Rica (Sallarès, 1999).

derive the local features of the 3-D velocity field within this layer and at the deeper ones.

8. Discussion

As shown in Fig. 4, one of the most significant features of the averaged velocity field beneath the isthmus is the presence of low velocity material within the upper mantle. Since most of the local earthquakes used to invert this velocity model are located in the central part of the isthmus (Fig. 3), we infer that the low velocity material must be compelled, at least, in this central part. As shown in Fig. 10, the 1-D tomographic results are compatible with those obtained from seismic refraction in the northernmost part of the Costarican isthmus (Sallarès, 1999). This suggests that, in general terms, velocities and particularities inferred by seismic tomography in the central part can be extrapolated to all the northern half of the isthmus (from the NW–SE seismic alignment to the north of the Nicoya Peninsula).

The synthesis of the most meaningful structural characteristics of the northern and southern parts of the isthmus is thus as follows. The northern part is seismically and magmatically active, is characterized by a sequence of small-scale (<20 km) and prominent velocity anomalies and shows a certain accumulation of low velocity material (7.4–7.5 km/s) within the upper mantle. The southern part is seismically less active, shows a volcanic gap, and the velocity field is much more homogeneous.

The differences in the crustal structure of the subducting slab and in the geometry of subduction have a major influence in the geochemical evolution of the subducting and overlying plates. The first processes of metamorphic dehydration of the oceanic crustal rocks are known to begin below 80–100 km depth (Wilson, 1989). The high-pressure water vapor originated by the metamorphic transformations induces partial melting of subducted sediments and asthenospheric material (i.e. pyrolite), producing basaltic magmas. These magmas ascend through the upper mantle by convection and accumulate progressively at the base of the overlying crust. The fluids released are also thought to cause serpentinization of mantle peridotites, forming hydrated mineral phases (serpentinite, chlorite) which are considerably less dense than peridotite (Peacock, 1987; Ponko and Peacock, 1995). Both processes together contribute to diminish substantially the upper mantle velocity and density, as observed, for example, in Alaska (Kissling and Lahr, 1991) or the Aleutian (Fliedner and Klemperer, 1999) and Ryuku (Iwasaki et al., 1990) island arcs. The basaltic magmas can fractionate as they ascend and intrude the overlying crust, provoking the thickening of the lower crustal levels (the less volatile components; i.e. mafic granulites), the magmatic intracrustal intrusions, and the extrusion of the more volatile components, as andesites (Holbrook et al., 1992; Rudnick and Jackson, 1995). Occurrence of crystal fractionation beneath the Costarican isthmus is reflected in the composition of magmas which are erupted nowadays in the volcanic arc (Kussmaul et al., 1994).

We suggest that most of the structural differences

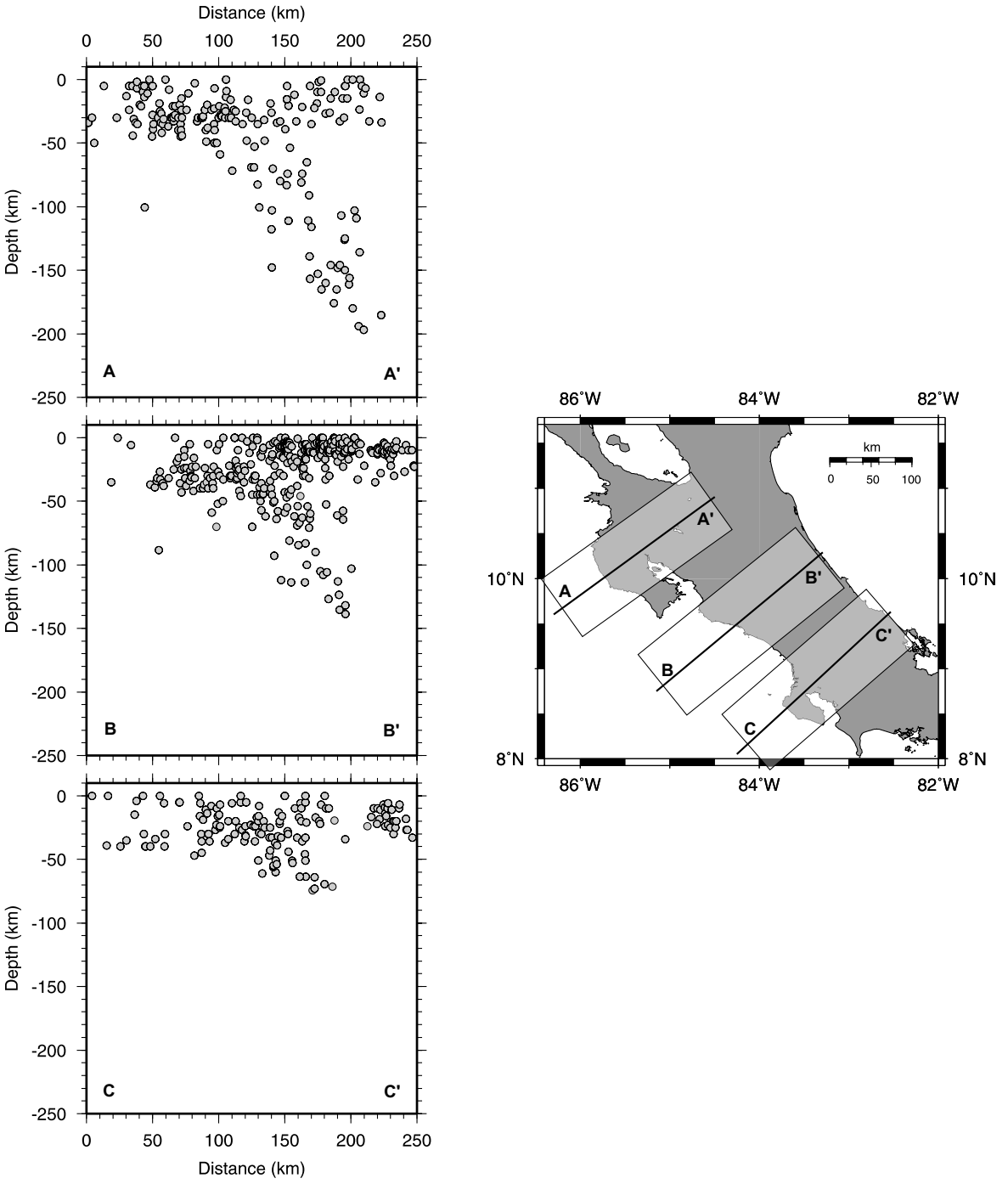

Fig. 11. Cross-sections of seismic activity across the three provinces defined within the Costarican isthmus (Von Huene et al., 1995): A–A′ (Nicoya Peninsula); B–B′ (Quepos segment); C–C′ (Cocos Ridge).

between northern and southern segments of the Costarican isthmus can be qualitatively explained by this scheme. The segment of the Cocos plate subducting north from the Osa Peninsula is typically oceanic (the Nicoya Peninsula segment) or slightly thickened (the Quepos segment) (Von Huene et al., 1995). Thus, the dip angle is considerably high in both segments, and the deepest subduction-related earthquakes are located at 200 km in the Nicoya Peninsula and around 150 km in the Quepos segment (Protti et al., 1995) (Fig. 11). This means that there are adequate conditions to originate basaltic magmas within the asthenosphere, and their existence is reflected in the upper mantle velocities (7.4–7.5 km/s). Crystal fractionation of these magmas is estimated to provoke a progressive thickening of the lowermost crustal levels of the overlying plate since the onset of subduction, ~75 Ma ago (Burke, 1988). This would explain qualitatively the crustal thickness of the isthmus (~40 km) to be about twice the averaged thickness of the Caribbean plateau (~20 km). Moreover, lowermost crustal seismic velocities (~7.1 km/s) are also compatible with those described for a lower crust composed essentially by mafic granulites (see, for e.g. Holbrook et al., 1992). The remnant of the magmas ascended through the crust, causing magmatic intrusions, which are represented by the small-scale heterogeneities in the velocity field, and inducing most of the intracrustal seismicity. Finally, the last components of the magmas are extruded at the surface, building up the volcanic edifice.

In contrast, the Cocos Ridge subducting below the Osa Peninsula has been extremely overthickened by Galápagos hotspot-derived material. Hence, this segment of oceanic crust is more buoyant, and the induced angle of subduction is much lower, being the deepest subduction-related earthquakes located above 70 km (Fig. 11). Consequently, the subducting plate does not become dehydrated, and partial melting of asthenospheric material does hence not occur. The lack of basaltic magmas intruding the crust is revealed by the homogeneous velocity field, which characterizes this part of the isthmus, as well as by the scarce intracrustal seismicity and the gap in the volcanic arc. Unfortunately, little is known about the deep crustal structure of this part of the isthmus. Stavenhagen et al. (1998) derived a 2-D velocity-depth model from refraction data. Their model is well defined at upper and mid crustal levels (above 20 km depth) but the deeper levels are not well resolved by the data. However, they argued the existence of an 'atypical' lower crust ($v \leq 7.2$ km/s) in which most of the intracrustal seismicity happens. This layer would correspond to our Layer 5 (Fig. 9e), though we suggest that both the seismicity and the associated high velocity anomaly could be the expression of the Cocos Ridge subduction. Nevertheless, any interpretations remain speculative. In any case, it is necessary to determine more exactly the deep crustal structure and the crustal thickness of this part of the isthmus in order to reveal its nature and origin.

9. Conclusions

This work shows that most of the structural differences between the northern and southern segments of the lithosphere beneath the Costarican isthmus can be explained by the lateral variations in the geometry (and structure) of the Cocos plate. The main parameter controlling the evolution of structure of the overlying plate in the subduction zone is suggested to be the dip angle of subduction, which is closely related with the crustal thickness. Thus, the oceanic crust subducting beneath the northern part of the isthmus, located to the north of a SW–NE seismic alignment, shows a steep subduction angle with subduction-related seismic activity below 150 km depth. This allows metamorphic dehydration processes to occur within the subducted crust, and the released fluids can induce the formation of basaltic magmas within the asthenosphere. The low seismic velocities inverted within the upper mantle reveal the presence of these magmas. Crystal fractionation of the basaltic magmas as they ascend through the crust is thought to have produced thickening of the overlying crust, intracrustal magmatic intrusions and the induced seismicity. The overthickened oceanic crust subducting south from the seismic alignment shows a lower dip angle, being the lowermost subduction-related earthquakes located above 60 km depth. Thus, in this crustal segment, dehydration of crustal rocks does not take place, and basaltic magmas are not generated. This is revealed by the gap in the volcanic arc, the drastic diminishing of intracrustal seismicity

and the homogeneity of the velocity field. However, more information is needed to determine the crustal thickness and upper mantle velocities in order to compare it with the northern segment.

Acknowledgements

The research for this paper was supported by EU project #CT94-0078 funding the first author scholarship (V. Sallarès). Additional funds came from CIRIT (project 1997SGR00020). Special thanks to Mario Villagrán (CEPREDENAC) and Ileana Boschini (ICE) for providing the local earthquakes data set. We are also grateful to E. Kissling for his inestimable help with the simultaneous inversion scheme philosophy. The comments and corrections from J. Mezcua helped to improve substantially the original manuscript.

References

Alvarado, G.E., Denyer, P., Sinton, C.W., 1997. The 89 Ma Tortugal komatiitic suite, Costa Rica: implications for a common origin of the Caribbean and Eastern Pacific region from a mantle plume. Geology 25 (5), 439–442.

Astorga, A., Fernández, J.A., Barboza, G., Campos, L., Obando, J., Aguilar, A., Obando, L.G., 1991. Cuencas sedimentarias de Costa Rica: Evolución geodinámica y potencial de hidrocarburos. Rev. Geol. Am. Central 13, 25–59.

Barckhausen, U., Roeser, H.A., von Huene, R., 1998. Magnetic signature of upper plate structures and subducting seamounts at the convergent margin off Costa Rica. J. Geophys.Res. 103, 7079–7093.

Berrangé, J.P., Thorpe, R.S., 1988. The geology, geochemistry and emplacement of the Cretaceous–Tertiary ophiolitic Nicoya Complex of the Osa Peninsula, southern Costa Rica. Tectonophysics 147, 193–220.

Bowland, C.L., Rosencrantz, E., 1988. Upper crustal structure of the western Colombian Basin, Caribbean Sea. Geol. Soc. Am. Bull. 100, 534–546.

Burbach, G.V., Frohlich, C., Pennington, W.D., Matumoto, T., 1984. Seismicity and tectonics of the subducted Cocos Plate. J. Geophys. Res. 89 (9), 7719–7735.

Burke, K., 1988. Tectonic evolution of the Caribbean. Ann. Rev. Earth Planet. Sci. 16, 201–230.

Colombo, D., 1995. Tomografia Sismica ed analisi sismotettonica della Costa Rica centrale. PhD thesis. Dipartim. di Scienze della Terra (Univ. Milano), Milano, 153 pp.

Corrigan, J., Mann, P., Ingle, J.C., 1990. Forearc response to subduction of the Cocos Ridge, Panamá-Costa Rica. Geol. Soc. Am. Bull. 102, 628–652.

Dañobeitia, J.J., Sallarès, V., Gallart, J., 1998. Local earthquakes tomography in the Betic Cordillera (Southern Spain). Earth Planet. Sci. Lett. 160, 225–239.

Donnelly, T.W., 1994. The Caribbean Cretaceous basalt association: a vast igneous province that includes the Nicoya Complex of Costa Rica. Profil. 7 (Univ. Stuttgart), pp. 17–45.

Duncan, R.A., Heargraves, R.B., 1984. Plate tectonic evolution of the Caribbean region in the mantle reference frame. Geol. Soc. Am. Mem. 162, 81–93.

Eberhart-Phillips, D., 1986. Three-dimensional velocity structure in northern California Coast Ranges from inversion of local earthquakes arrival times. Bull. Seismol. Soc Am. 76, 1026–1032.

Fisher, R.L., 1961. Middle American Trench: topography and structure. Geol. Soc. Am. Bull. 72, 703–720.

Frisch, W., Meschede, M., Sick, M., 1992. Origin of the Central America ophiolites: evidence from paleomagnetic results. Geol. Soc. Am. Bull. 104, 1301–1314.

Gardner, T.W., Verdonck, D., Pinter, N.M., Slingerland, R., Furlong, K.P., Bullard, T.F., Wells, S.G., 1992. Quaternary uplift astride the aseismic Cocos Ridge, Pacific coast, Costa Rica. Geol. Soc. Am. Bull. 104, 219–232.

Goedde, H., Mechie, J., Schulze, A., 1997. Geological interpretation of wide-angle seismic measurements at the Pacific margin of Costa Rica. AGU Fall Meeting 1997, pp. T12A-6.

Gomberg, J.S., Sheldock, K.M., Roecker, S.W., 1990. The effect of S-wave arrival times on the accuracy of hypocenter estimations. Bull. Seismol. Soc. Am. 80, 1605–1628.

Güendel, F., McNally, K.C., Lower, J., Protti, M., Sáenz, R., Malavassi, E., Barquero, J., Van der Laat, R., González, V., Montero, C., Fernández, E., Rojas, D., Segura, J., Mata, A., SolÍs, Y., 1989. First results from a new seismographic network in Costa Rica, Central America. Bull. Seismol. Soc. Am. 79, 205–210.

Gursky, H.J., 1988. Gefüge, Zusammensetzung und Genese der Radiolarite im ophiolitischen Nicoya-Komplex (Costa Rica). Münster. Forsch. Geol. Paläontol. 68, 1–189.

Hauff, F., Hoernle, K., Schmincke, H.-U., Werner, R., 1997. A Mid Cretaceous origin for the Galápagos hotspot: volcanological, petrological and geochemical evidence from Costa Rican oceanic crustal segments. Geol. Rundsch. 86, 141–155.

Hey, R., 1977. Tectonic evolution of the Cocos-Nazca spreading center. Geol. Soc. Am. Bull. 88, 1404–1420.

Hill, R.I., 1993. Mantle plumes and continental tectonics. Lithos 30, 193–206.

Hinz, K., von Huene, R., Ranero, C., 1996. Tectonic structure of the convergent Pacific margin offshore Costa Rica from multichannel seismic reflection data. Tectonics 15 (1), 54–66.

Holbrook, W.S., Mooney, W.D., Christensen, N.I., 1992. The seismic velocity structure of the deep continental crust. In: Fountain, D.M., Arculus, R., Kay, R.W. (Eds.), Continental Lower Crust. Elsevier, Amsterdam, pp. 1–34.

Iwasaki, T., Hirata, N., Kanazawa, T., Melles, J., Suyehiro, K., Urabe, T., Möller, L., Makris, J., Shimamura, H., 1990. Crustal and upper mantle structure in the Ryukyu Island Arc deduced from deep seismic sounding. Geophys. J. Int. 102, 631–651.

Kissling, E., 1988. Geotomography with local earthquake data. Rev. Geophys. 26, 659–698.

Kissling, E., Lahr, J.C., 1991. Tomographic image of the

Pacific slab under southern Alaska. Eclogae Geol. Helv. 84, 297–315.

Kissling, E., Ellsworth, W.L., Eberhart-Phillips, D., Kradolfer, U., 1994. Initial reference models in local earthquake tomography. J. Geophys. Res. 99 (10), 19 635–19 646.

Kussmaul, S., Tournon, J., Alvarado, G., 1994. Evolution of the Neogene to Quaternary igneous rocks of Costa Rica. Profil 7 (Univ. Stuttgart), pp. 97–123.

Longsdale, P., Klitgord, K.D., 1978. Structure and tectonic history of the Eastern Panamá Basin. Geol. Soc. Am. Bull. 89, 981–999.

Lundberg, N., 1991. Detrital record of the early Central American magmatic arc: petrography of intraoceanic forearc sandstones, Nicoya Peninsula, Costa Rica. Geol. Soc. Am. Bull. 103, 905–915.

Matumoto, T., Othake, M., Latham, G., Umaña, J., 1977. Crustal structure of southern Central America. Bull. Seismol. Soc. Am. 67, 121–134.

Pavlis, G.L., Booker, J.R., 1980. The mixed discrete-continuous inverse problem: application to the simultaneous determination of earthquake hypocenters and velocity structure. J. Geophys. Res. 85 (9), 4801–4810.

Peacock, S.M., 1987. Thermal effect of metamorphic fluids in subduction zones. Geology 15, 1057–1060.

Pindell, J.L., Barrett, S.F., 1990. Geological evolution of the Caribbean region; a plate-tectonic perspective. In: Dengo, G., Case, J.E. (Eds.), The Geology of North America, Volume H: The Caribbean Region. Geological Society of America, Boulder, CO, pp. 405–432.

Ponko, S.C., Peacock, S.M., 1995. Thermal modeling of the southern Alaska subduction zone: insight into the petrology of the subducting slab and overlying mantle wedge. J. Geophys. Res. 100 (B11), 22 117–22 228.

Protti, M., Güendel, F., McNally, K., 1995. Correlation between the age of the subducting Cocos plate and the geometry of the Wadati-Benioff zone under Nicaragua and Costa Rica. Geol. Soc. Am. Spec. Paper 295, 309–326.

Richards, M.A., Duncan, R.A., Courtillot, V.E., 1989. Flood basalts and hot-spot tracks: plume heads and tails. Science 246, 103–107.

Rudnick, R.L., Jackson, I.N.S., 1995. Measured and calculated elastic wave speeds in partially equilibrated mafic granulite xenolits: implications for the properties of an underplated lower continental crust. J. Geophys. Res. 100, 10 211–10 218.

Sallarès, V., 1999. Lithospheric structure of the Costa Rica Isthmus (Central America): effects of magmatism at the convergent margin of an oceanic plateau. PhD thesis. Univ. Barcelona, Barcelona, 230 pp.

Sallarès, V., Dañobeitia, J.J., Flueh, E.R., Leandro, G., 1999. Seismic velocity structure across the Middle American Landbridge in Northern Costa Rica. J. Geodyn. 27, 327–344.

Sinton, C.W., Duncan, R.A., Denyer, P., 1997. The Nicoya Peninsula, Costa Rica: a single suite of Caribbean oceanic plateau magmas. J. Geophys. Res. 102, 15 507–15 520.

Sinton, C.W., Duncan, R.A., Storey, M., Lewis, J., Estrada, J.J., 1998. An oceanic flood basalt province within the Caribbean plate. Earth Planet. Sci. Lett. 155, 221–235.

Solarino, S., Kissling, E., Sellami, S., Smriglio, G., Thouvenot, F., Granet, M., Bonjer, K.P., Sleijko, D., 1997. Compilation of a recent seismicity data base of the greater Alpine region from several seismological networks and preliminary 3D tomographic results. Ann. Geofis. XL (1), 161–174.

Stavenhagen, A., Flueh, E.R., Ranero, C., McIntosh, K., Shipley, T., Leandro, G., Schulze, A., Dañobeitia, J.J., 1998. Seismic wide-angle investigations in Costa Rica — a crustal velocity model from the Pacific to the Caribbean coast. Zbl. Geol. Paleontol. 3–6, 393–406.

Thurber, C.H., 1983. Earthquakes locations and three-dimensional crustal structure in the Coyote Lake area, central California. J. Geophys. Res. 88, 8226–8236.

Thurber, C.H., 1992. Hypocenter-velocity structure coupling in local earthquake tomography. Phys. Earth Planet. Inter. 75, 55–62.

Tournon, J., Alvarado, G., 1997. Carte Géologique du Costa Rica-Mapa Geológico de Costa Rica. Notice Explicative-Folleto Explicativo, escala 1:500.000. Editorial Tecnológica de Costa Rica, 80 pp.

Um, J., Thurber, C.H., 1987. A fast algorithm for two-point seismic ray tracing. Bull. Seism. Soc. Am. 61, 729–746.

Von Huene, R., Bialas, J., Flueh, E., Cropp, B., Csernok, T., Fabel, E., Hoffmann, J., Emeis, K., Holler, P., Jeschke, G., Leandro, C., Pérez, I., Chavarria, J., Florez, A., Escobedo, Z., León, R., Barrios, O., 1995. Morphotectonics of the Pacific convergent margin of Costa Rica. Geol. Soc. Am. Spec. Paper 295, 291–307.

Von Huene, R., Ranero, C.R., Weinrebe, W., Hinz, K., 1999. Quaternary convergent margin tectonics of Costa Rica, segmentation of the Cocos plate, and Central American volcanism. Submitted for publication.

Werner, R., Hoernle, K., van den Bogaard, P., Ranero, C.R., von Huene, R., Korich, D., 1999. Drowned 14 M.y. old Galapagos archipelago off the coast of Costa Rica: implications for tectonic and evolutionary models. Geology 27 (6), 499–502.

Wildberg, H., 1984. Die Nicoya-Komplex, Costa Rica, Zentralamerika: Magmatismus und Genese eines polygenetischen Ophiolith-Komplexes. Münster Forsch. Geol. Paläontol. 62, 1–123.

Wilson, J.T., 1989. Igneous Petrogenesis. A Global Teconic Approach. Unwin Hyman, London.

Ye, S., Bialas, J., Flueh, E.R., Stavenhagen, A., von Huene, R., Leandro, G., Hinz, K., 1996. Crustal structure of the Middle American Trench off Costa Rica from wide-angle seismic data. Tectonics 15 (5), 1006–1021.